The Influence of Bed Roughness on Turbulence: Cabras Lagoon, Sardinia, Italy

Clémentine Chirol, Carl Amos, Hachem Kassem, Alice Lefebvre, Andrea Cucco, Georg Umgiesser

J. Mar. Sci. Eng. **2015**, *3*, 935-956; doi:10.3390/jmse3030935

OPEN ACCESS

Journal of
Marine Science and Engineering
ISSN 2077-1312
www.mdpi.com/journal/jmse

Article

The Influence of Bed Roughness on Turbulence: Cabras Lagoon, Sardinia, Italy

Clémentine Chirol [1,*], Carl L. Amos [1], Hachem Kassem [1], Alice Lefebvre [2], Georg Umgiesser [3] and Andrea Cucco [4]

[1] Ocean and Earth Sciences Department, National Oceanography Centre Southampton, Southampton SO14 3ZH, UK; E-Mails: cla8@noc.soton.ac.uk (C.L.A.); Hachem.Kassem@soton.ac.uk (H.K.)
[2] MARUM Centre for Marine Environmental Sciences, University of Bremen, Bremen D-28334, Germany; E-Mail: alefebvre@marum.de
[3] Institute of Marine Science ISMAR, National Research Council, Lanusei (OG) 08045, Italy; E-Mail: georg.umgiesser@ismar.cnr.it
[4] Institute for coastal marine environment (IAMC), National Research Council, Oristano (IT) 09170, Italy; E-Mail: andrea.cucco@cnr.it

* Author to whom correspondence should be addressed; E-Mail: cc4v12@soton.ac.uk; Tel.: +44-23-8059-24786.

Academic Editor: Charitha Pattiaratchi

Received: 9 June 2015 / Accepted: 11 August 2015 / Published: 19 August 2015

Abstract: Estimates of bed roughness used for predictions of sediment transport are usually derived either from simple scalars of the physical roughness (*i.e.*, ripple height or grain size) or from the hydrodynamic roughness length (Zo) based upon velocity gradient estimates in the benthic boundary layer. Neither parameter accounts for irregular bed features. This study re-evaluates the relation between hydrodynamic roughness and physical bed roughness using high-resolution seabed scanning in the inlet of a shallow lagoon. The statistically-robust relationship, based on a 1D statistical analysis of the seabed elevation at different locations of the Cabras lagoon. Sardinia, has been obtained between Zo and the topographical bed roughness Ks by defining Ks = 2*STD + skin friction, with STD the standard deviation of the seabed elevation variations. This correlation between Ks and Zo demonstrates that the roughness length is directly influenced by irregular bed features, and that the Reynolds number accounts for the total drag of the bed: the data points collapse on the Law of the Wall

curves with a fitting factor $x = 0.5$. Further testing must be done in other locations and in the fully-rough domain in order to test how widely those new parameters can be applied.

Keywords: turbulence; bed roughness; small-scale topography; roughness length; Law of the Wall

1. Introduction

The benthic boundary layer is the portion of the water column that is directly affected by bed frictional drag [1,2]. In the coastal region, this layer plays an important role in the dynamics and biochemistry of ecosystems [3], and has a number of applications in fields such as marine engineering, meteorology, and oceanography [4]. However, our understanding of turbulence in the benthic boundary layer is complicated by the lack of a reliable equation for the drag caused by the pressure differences at the sediment-water interface [5,6].

The stress applied to the bed in this layer depends on a number of factors: the flow characteristics, the suspended sediment concentration [6–9], and the irregularities of the bed [10]. Energy dissipation caused by the suspended sediment is significant even at low concentrations [9]. However, in the case of a concentration lower than 200 mg/L (such as Cabras lagoon), only the physical roughness is considered to influence drag in the benthic boundary layer.

The relationship between hydrodynamic drag in a benthic boundary layer and the physical roughness of the benthos in the natural environment is crude. One relies heavily on scalar quantities such as the roughness length (Zo), drag coefficient (Cs), and friction factor (*f*) to estimate bed shear stress [4,5]. Such quantities are inferred from the hydrodynamics of the studied site: they do not depend on the sediment properties or on the topography of the bed. However, in shallow coastal regions, irregularities of the bed have a major impact on the flow in the benthic boundary layer [4].

The topographical bed roughness, Ks, may be defined as the extent to which the seabed deviates from a perfectly planar surface and modifies the overlying fluid flow [11]. It has been assumed that only the skin friction (due to the resistance of the particles forming the bed and controlled by grain size) is important for studying the turbulent state, while other studies consider the total stress, which is the sum of the skin friction and form drag; the additional shear stress is due to the irregularities of the bed [10,12].

Of particular interest is the small-scale asperity, from 10^{-2} to 10^{-1} meters, which has a significant influence on boundary layer dynamics [13]. This contribution to roughness is less stable than large-scale features and may be composed of ripples generated by waves and currents as well as biologically-generated topography. The locomotion and feeding activity of animals can leave trails and burrows that influence the bed roughness. The presence of small reefs or shells may also influence the topography.

For regular bed features, such as ripples, relations between bed roughness and the dimensions of the roughness elements have been extensively studied [14]. However, in the case of heterogeneous beds, the estimation of the bed roughness is arbitrary. The lack of a quantitative, reproducible estimate of the topographical bed roughness limits the reliability of hydrodynamic models in shallow coastal areas.

One objective of this study is to quantitatively define the topographical bed roughness at a variety of locations in the Cabras lagoon, Sardinia. A commonly used Ks parameter is the equivalent Nikuradse

bed roughness. The parameter is linked to the hydrodynamic roughness length Zo, the height at which the mean velocity is zero, by the following relation [15]:

$$\mathrm{Zo} = \frac{\mathrm{Ks}}{30} \tag{1}$$

This equation is valid for pipe flow experiments where grains of equal size are glued to the smooth walls of the pipe [16]. The validity of this relation in the case of field data, where topography is present and where the bed is heterogeneous, is doubtful.

Validation of a given relationship will be tested using the Reynolds number, a dimensionless indicator of the flow state, of which many definitions exist. The one found in Clauser [4] is:

$$\mathrm{Re} = \frac{\mathrm{U}* \mathrm{D}}{\nu} \tag{2}$$

where U* is the friction velocity, ν the kinematic viscosity of the fluid [17], and D, a length scale, often equated with the height of the measurement Z. This definition can be simplified by including the roughness length [18]:

$$\mathrm{Zo} = \frac{\nu}{xU*} \tag{3}$$

where x is an empirical coefficient. According to laboratory experiments for smooth turbulent flows, x = 9; this value however does not necessarily apply to shallow water marine conditions [18]. Rearranging Equations (2) and (3) gives us a new definition of the Reynolds number [16,18]:

$$\mathrm{Re} = \frac{\mathrm{Z}}{x\mathrm{Zo}} \tag{4}$$

The Law of the Wall describes the logarithmic increase of velocity with height above the bed in the benthic boundary layer. The equations given by the Law of the Wall are derived from the slope and offset of the best fit curve for the two different turbulent states (Figure 1):

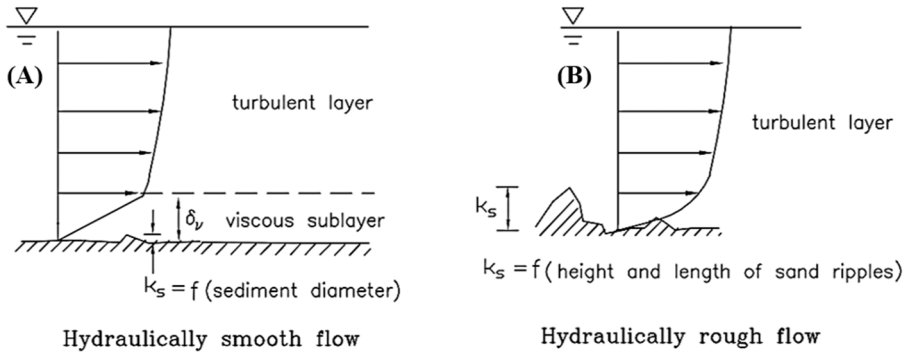

Figure 1. (**A**) Universal velocity distribution for turbulent layers near smooth walls; (**B**) Universal velocity distribution for turbulent layers near rough walls (modified from Liu [16]).

For hydraulically smooth flows, when the roughness elements are smaller than the viscous sublayer, the relation between the Reynolds number and the dimensionless velocity ($\bar{U}$/U*) is linear in the viscous sublayer:

$$\frac{\bar{\mathrm{U}}}{\mathrm{U}*} = \frac{\mathrm{Z}}{\mathrm{Zo}} \tag{5}$$

The relation is logarithmic in the fully turbulent part of the flow where κ is von Karman's constant:

$$\frac{\bar{U}}{U*} = \frac{1}{\kappa} \ln (Re) \quad (6)$$

Which gives, using our definition of the Reynolds number shown in Equation (4):

$$\frac{\bar{U}}{U*} = \frac{1}{\kappa} \ln \left(\frac{Z}{xZo}\right) \quad (7)$$

Equations (6) and (7), referred to as the Law of the Wall, are valid from the height of the roughness length, a few centimeters above the bed (a few millimeters in the case of a flat muddy bed), to about 20%–30% of the water depth [18]. When the mean flow and Reynolds number increase, the flow in the boundary layer evolves from turbulent smooth to turbulent rough, and the roughness elements are larger than the viscous sublayer, thus affecting the velocity profile.

The Law of the Wall was first demonstrated in laboratory experiments, where the empirical coefficient $x = 9$ [18]. However, field experiments have found this value to be extremely variable, ranging between 4 and 272 for unidirectional steady flows at a water depth of about 100 m, with no visible bedforms [18,19].

Previous studies have explored the correlation between the flow field and the morphology of the bed in the Po River [20], but at too large a scale to infer anything about the turbulent state. This study explores the applicability of the Law of the Wall to field data with various small-scale bed features, and evaluates the effect of compound bed roughness on the flow turbulent state in the lower part of the benthic boundary layer. A length scale will be extracted from an analysis of quantitative topographical bed roughness, which considers bed elevations as a three-dimensional random field, as explored in previous studies [21–24]. This length scale will be compared with the hydrodynamic roughness length Zo in order to evaluate the applicability of the Nikuradse relation to field data. The data will then be evaluated on a Clauser plot to compare field data over compound roughnesses to previously published results over standard beds.

2. Methods

2.1. Study Site

Cabras lagoon is situated near the city of Oristano in Western Sardinia, Italy (Figure 2). It is dominated by semi-diurnal tidal currents and wind-induced standing waves of a period of 15 min. It is the largest basin of brackish water in Sardinia, occupying an area of 22.28 km^2; this shallow lagoon has an average depth of 1.6 m and a maximum depth of 2.1 m [25]. The extensive fishery in Cabras lagoon makes it a zone of high economic and environmental significance.

Eight stations of varying bottom roughness and flow conditions were occupied in this study. They were situated in the outlet of Cabras lagoon, which connects with the Gulf of Oristano (Figure 2). The outlet has been modified by man-made structures including an inlet gate, a road bridge, flood protection dykes, and fish barriers. The gate was built at the high-tide level a few decades ago to maintain the lagoon at a constant water level [26]. As a result, the current velocities induced by the tide are very weak: the tidal amplitude is less than 25 cm [27]. The water circulation is, thus, dominantly wind-driven [28].

Cabras lagoon is subjected to three typical wind regimes: the Mistral blowing from the NW, the Libeccio from the SW, and the Sirocco from the SE. Models comparing the effect of these winds

with a purely tidal regime have shown that the Mistral is the driving factor for the hydrodynamic activity of the lagoon [25]. This has an impact on the sediment distribution in the study site. Indeed, the western side of the outlet, where stations 1 to 5 of this study are located, is characterized by shelly mud, while the eastern side, where stations 8 to 10 are located, is subjected to stronger winds and contains a larger fraction of sand.

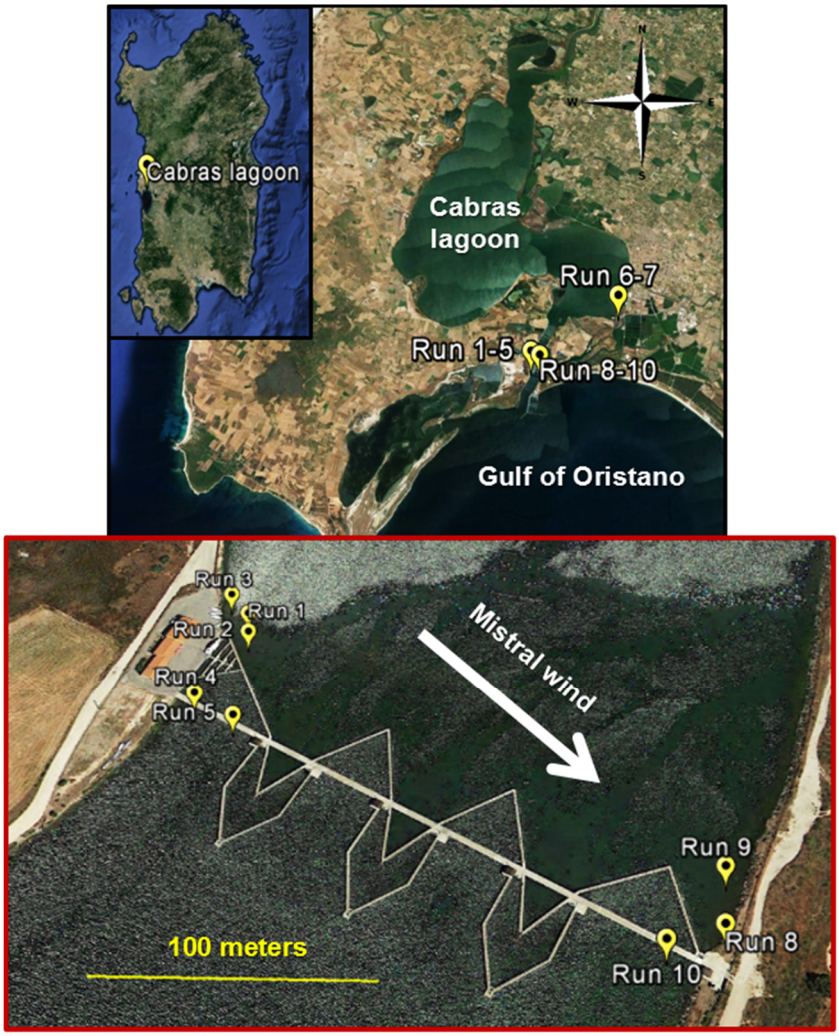

Figure 2. Station locations and dominant wind regime (modified from Google Earth). The road bridge across the inlet, and the (zig-zag) fish weirs are clearly seen in the close-up image, which excludes stations 6 and 7.

2.2. Topographical Bed Roughness Estimate Using BRAD

A field campaign was carried between the 15th and the 20th September 2013 to measure velocity profiles and three-dimensional (3D) images of the seabed and water column at 10 sites along the inlet at water depths of 1 to 3 m. (Figure 2). The occupied sites show a varied seabed topography with the presence of serpulid worm reefs, bioturbated muds, and seagrass (Figure 3). The seagrass canopy is present in patches at sites 8, 9, and possibly at site 10 (Figure 3). Two other deployments (stations 6 and 7) were made at the entrance of two secondary channels (Figure 2).

Since each site takes 90 min to survey, and since the flow shows some variation with time, replication of data collection was impossible. Deployment occurred once in each location, and the sites were then selected on the basis of data quality. In the case of stations 6 and 7, boulders on the bed and extremely turbulent flow resulted in poor quality data due to instrument instability and will not be included in the results.

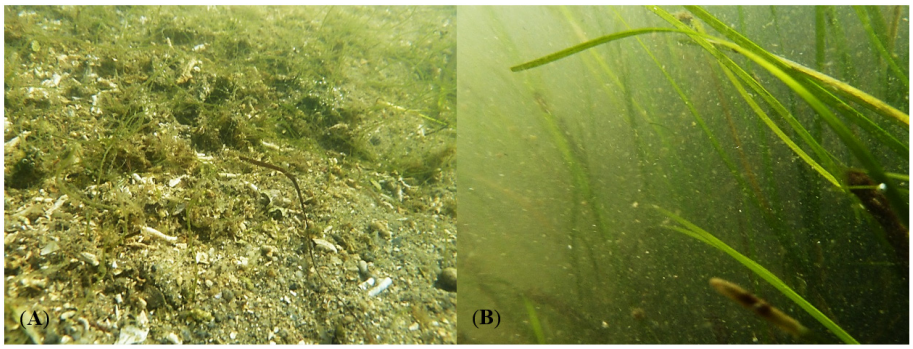

Figure 3. Two examples of the seabed near the study sites 8, 9, and 10; (**A**) serpulid tube fragments scattered over a sandy bed, with patches of seagrass, and (**B**) a seagrass bed of *Zostera marina*.

The position and characteristics of the bed for each site are described in Table 1. Since several factors besides bed roughness can influence the flow, including water depth, wind speed, and distance from the fish weirs, those characteristics are also summarized in the table.

Three-dimensional images of the seabed and water column were created to determine the topography using the Benthic Roughness Acoustic Device (BRAD). BRAD consists of a Sediment Imaging Sonar (SIS Marine Electronics Ltd, Guernsey, UK) mounted on a fixed frame that sits on the seabed. The SIS steps forward about 2 mm/sweep. The scanning section is 2 m by 0.94 m in size (Figure 4). The maximum area of seabed that can be scanned during one deployment is 1.7 m^2 [11]. During the 90 min of the survey, two Acoustic Doppler Velocimeters (ADVs) (Nortek Ltd., Providence, RI, USA) record flow in three dimensions continuously at 25 Hz at two different heights (Table 1). The two bars at the bottom of the frame stabilize BRAD and give a reference for image construction.

The SIS is fixed at a height of 0.88 m above the bed. Its rotating head emits a pencil-beam acoustic signal at a frequency of 1.1 MHz. The sonar sweeps 90° of arc centered on the nadir (pointing vertically down) as it moves along the frame. Scans are made at 0.9° of arc yielding about 100 beams per scan. About 15,000 beams are recorded over the 1.8 m of travel of the sonar. The backscatter intensity is determined by the reflection and scatter of suspended sediment, seagrass or the seabed. The normalized backscatter Q is defined as:

$$Q = \frac{Backscatter - Backscatter(water)}{Backscatter(\max) - Backscatter(water)} \quad (8)$$

where the backscatter value corresponding to the water column is empirically defined as the value measured between 0.5 and 0.6 m from the sensor head.

Table 1. A summary of the locations of BRAD sites and characteristics of the seabed. Also given are the heights of the two ADV sensors, the mean water depth, and the direction of travel of the SIS sensor head (Note this was considered important in the registration of the acoustical image to the frame of reference of the two ADV's).

Site	1	2	3	4	5	6	7	8	9	10
Latitude/Longitude	39°54.594′; 8°29.532′	39°54.588′; 8°29.533′	39°54.600′; 8°29.526′	39°54.570′; 8°29.520′	39°54.564′; 8°29.532′	39°55.080′; 8°31.139′	39°55.106′; 8°31.181′	39°54.516′; 8°29.660′	39°54.528′; 8°29.663′	39°54.513′; 8°29.645′
Water depth (m)	1.06	1.28	1.22	1.36	1.54	1.36	1.02	1.01	0.94	1.16
Wind speed (m/s) and direction	5.3 NW	7.2 NNW	8.2 NW	6.5 NNW	8.5 NW	8.2 NW	8.2 NW; (gust speed 17.5)	5.8 NW	9.4 NW; (gust speed 15.9)	10.1 NW; (gust speed 13.9)
Distance from inlet gate (>0 = *N* of weir) (m)	5	4	20	−7	−4	Not applicable	Not applicable	6	24	-6
Height of the upper ADV (m)	0.5	0.33	0.3	0.27	0.29	0.37	0.23	0.37	0.38	0.25
Height of the lower ADV (m)	0.32	0.14	0.01	0.011	0.17	0.2	0.05	0.18	0.08	0.08
Sense of SIS scanning	South-North	North-South	South-North	South-North	South-North	North East-South West	South West-North East	South West-North East	North-South	North-South
State of the tide	Ebb	Low tide	Flood	Ebb	Flood (Flow inward, wind blowing from West)	Ebb (Current to South, gusts of wind from the North, rain)	Low tide (Strong continuous flow to South)	Ebb	Ebb: BRAD half exposed by end of run	Ebb (water level deeper to the West. Wind from South West)
Suspended sediment (g/L)	0.01	0.04	0.03	0.01	0.02	0.04	0.06	0.06	0.03	0.08
General description of seabed	Shelly mud.	Shelly mud.	Shelly mud.	Shelly mud.	Shelly mud with serpulid reefs.	Sandy gravelly bed over silt. High turbidity. Floating algae. Serpulid reefs.	High turbidity. Floating algae. Serpulid reefs up to 15cm high and 40cm long.	Shelly sand. Patches of seagrass.	Shelly, sandy mud. Seagrass cover.	Shelly mud. Seagrass, turbidity too high to determine its density.

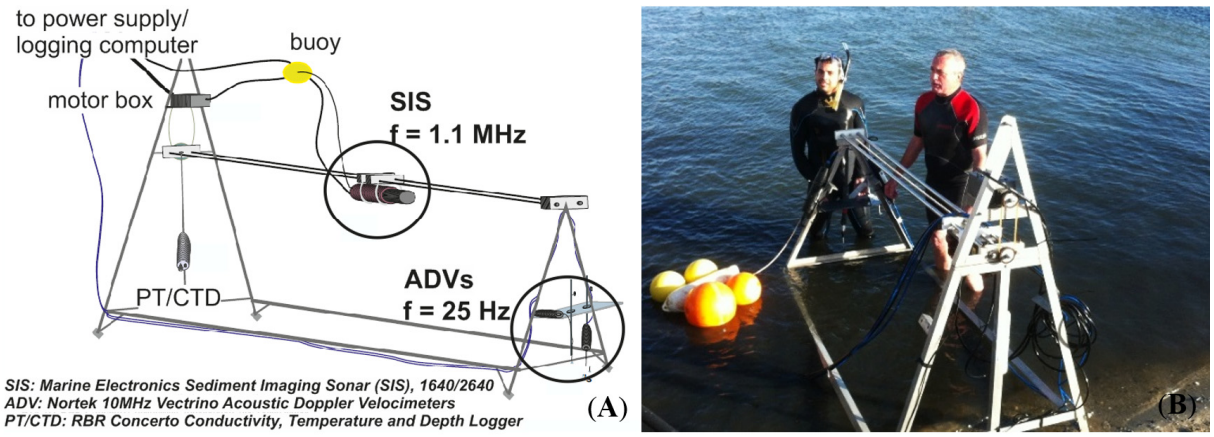

Figure 4. (**A**) A schematic of the BRAD device (modified from Lefebvre [11]); (**B**) The BRAD device on site.

The seabed is defined as the depth at which the normalized backscatter exceeds an empirically-found threshold of $Q = 0.81$. This value was defined by [11] based upon extensive sensitivity tests. Once the first estimation of the seabed position is made, a correction is applied for the backscatter attenuation with depth. The correction includes the attenuation due to water absorption, to scattering, and to viscosity [29]. The final output is a grid file of relative depth in x (along the frame) and y (across the frame) from which bed roughness is estimated. After corrections have been applied, the de-trended variations of topography are estimated from about 13,000 data points per site. Those points are first de-spiked using a phase-space method [30] as modified by Mori *et al.* [31], then linearly interpolated into a mesh of 507 × 507 points so the elevation can be plotted as a surface.

Subsections are selected to eliminate backscatter from the frame and to reduce edge effects. Histograms of relative elevation are used to derive statistical parameters of the topographical bed roughness using the method of moments. The number of data points is sufficient to confidently estimate first and second order statistical moments; that is to say, the mean and the standard deviation of the seabed elevation changes [32].

The size of the subsection used in the analyses varies between sites to avoid unwanted features such as footprints or instrument-related errors (tilting of the frame for example) in the seafloor mapping, as well as to avoid reflections from the frame of BRAD. In the case of Run 1, for instance, an error in data collection resulted in an abnormal shift in topography clearly visible at the bottom of the figure (Figure 5). The subsections should be representative of the topography of the study area. Ideally, the statistical parameters used to define bed roughness should be insensitive to the subsection size. In order to test this hypothesis, ten proportional subsections of the bed were extracted from the full data set at each station and the change in statistics of the topographical bed roughness was tested (Figure 6).

For most of the sites, the estimated roughness is unreliable below a subsection area of 0.4 m^2. Above this value, there is no significant change in the estimated topographical bed roughness (Figure 5). We suggest that scales up to 0.4 m^2 fall into the category of bed roughness and, hence, is likely to impact flow turbulence directly. In the case of topographic variations larger than 0.4 m^2, we consider that only the mean flow is affected (through continuity considerations) and thus do not contribute to bed roughness as defined herein.

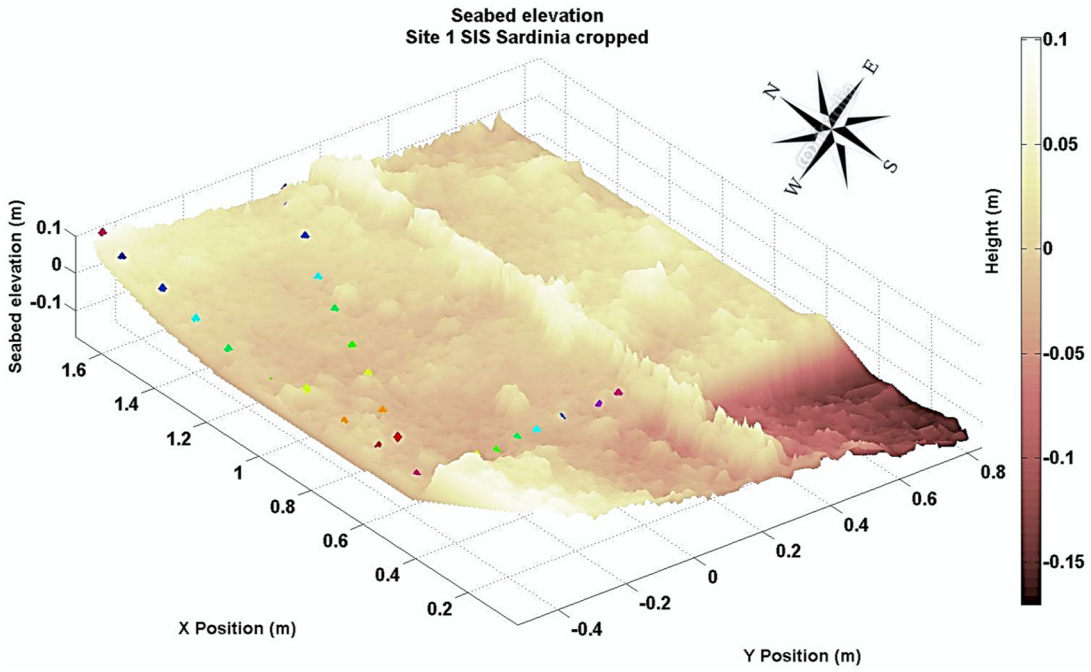

Figure 5. An example of the raw bed roughness from BRAD at station 1. The rectangular subsections of the bed where the topographical bed roughness is estimated are shown by the multi-colored dots in the figure.

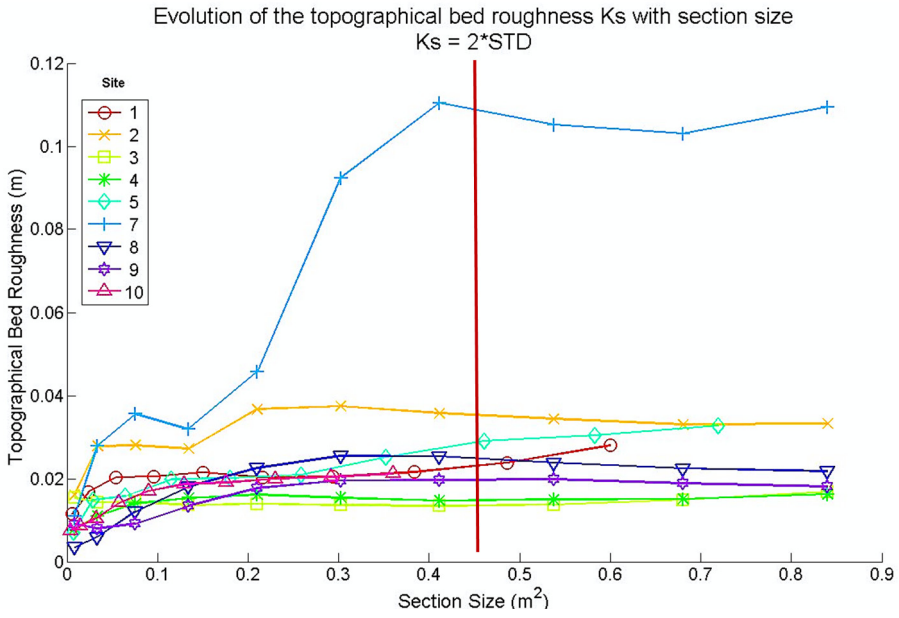

Figure 6. Standard deviation of the de-trended bed elevation variations (roughness) plotted against subsection areas for all sites of this study (Note site 7 has been included because it represents the greatest roughness and hence likely the most sensitive to changes in subsection size).

2.3. Roughness Length Zo Estimate

The roughness length Zo is defined as the intercept of the logarithmic velocity profile distribution [33]; that is to say, the depth at which the mean velocity is zero [34]. In order for the velocity

to be related to bed roughness, several conditions should apply: the flow must be fully developed, turbulent (or transitional), stationary, and uniform.

A CTD was added to the frame at a height of 0.45 m above the bed to measure the water depth, temperature, and salinity (Figure 3). Seawater density and viscosity were estimated from these measurements. Additionally, two Acoustic Doppler Velocimeters (ADVs) were fitted to the frame at two heights above the bed to measure mean current velocity and turbulence within the benthic boundary layer of the surveyed sites (Table 1).

The ADV record data in three orthogonal directions: streamwise (*U*, also parallel to the long axis of BRAD), crosswise (*V*), and vertical (*W*). Several data processing steps were undertaken to define the mean flow velocity at each height and of the turbulent fluctuations (using the Reynolds decomposition $U(t) = \overline{U} + U'$). This includes the elimination of data when the (Doppler) noise from the sensor is higher than 1% of the maximum velocity range, a rotation algorithm to correct for any sensor's misalignment with the peak flow, and a de-spiking algorithm to remove outliers based on a phase-space method [30] as modified by Mori *et al.* [31].

Corrected datasets have an approximate length of eighty minutes. The hypothesis of a uniform flow is reasonable considering the nearly constant value of crosswise and vertical velocities (Figure 7). However, variations in streamwise mean flow are evident throughout the time series, which means that the stationary flow hypothesis does not apply to the entire data set. To mitigate this variability, the time series is divided semi-automatically into eight minute intervals for which the flow is considered to be quasi-stationary. This has the advantage of providing a series of data sets (Reynolds numbers) at each location. The ADV time series of each data set contains 7500 data points, which is enough to estimate the mean and the standard deviation of the fluctuating flow [32].

The resultant of the mean velocity in the three directions is referred to as $\overline{U}$ and is found for each data point using the equation:

$$\overline{U} = \sqrt{U^2 + V^2 + W^2} \tag{9}$$

The resulting friction velocity is found using the turbulent kinetic energy method [35]. In the following equation we call E the kinetic energy:

$$E = \frac{1}{2}\rho(U'^2 + V'^2 + W'^2) \tag{10}$$

with *U'*, *V'*, and *W'* the friction velocity in the three directions. We define the friction velocity as the variation of the instantaneous velocity from the mean velocity for each data point ($U' = U - \overline{U}$). The kinetic energy is used to infer the stress τ:

$$\tau = 0.19 * E \tag{11}$$

The stress value figures in the following definition of the friction velocity:

$$U* = \sqrt{\frac{\tau}{\rho}} \tag{12}$$

The following allows us to calculate the resultant friction velocity from the ADV data:

$$U* = \sqrt{0.5 * 0.19 * (U - \overline{U})^2 + (V - \overline{V})^2 + (W - \overline{W})^2} \tag{13}$$

The roughness length Zo is found for each data point by plotting $\overline{U}$ at the two depths of measurement. A log-linear fit is extrapolated from the two points to find the depth at which $\overline{U} = 0$. This assumes a log-linear relationship in the lower part of the boundary layer, typical of turbulent flows. A linear fit is then made between Zo and Ks in order to check whether the Nikuradse relation holds for a heterogeneous bed. Zo is also used to plot the field data on the Clauser plot and see how well they follow the Law of the Wall.

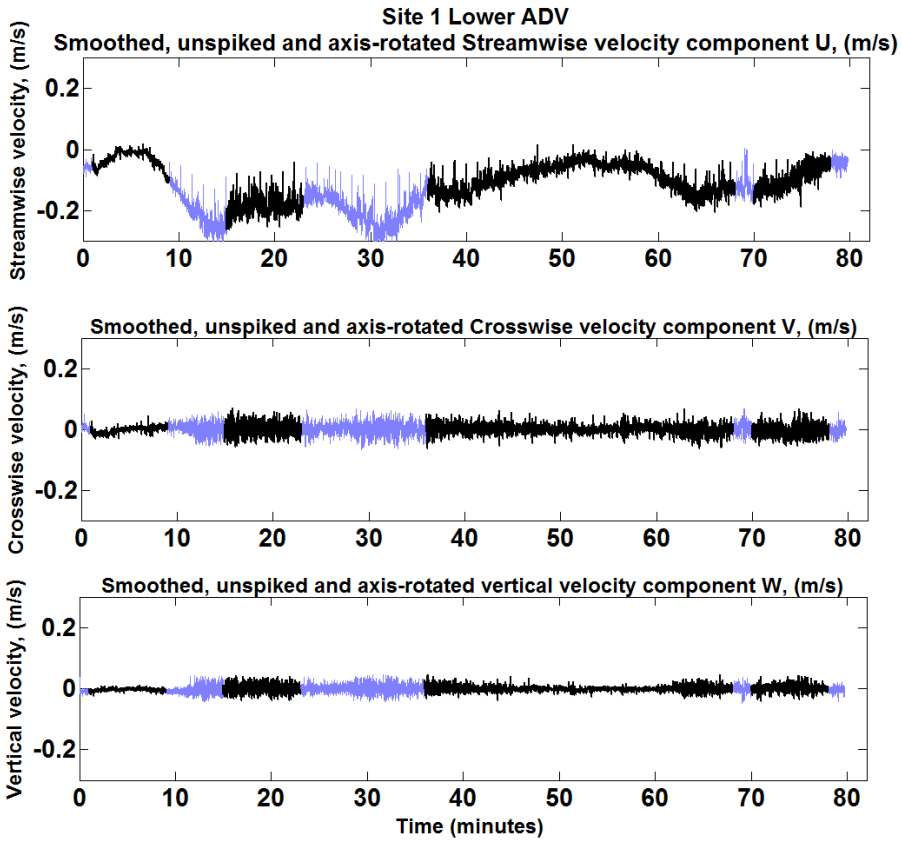

Figure 7. Eight minute sections selected in black for the lower ADV of site 1 (0.32 m above seabed). For each section the mean velocity $\overline{U}$, the turbulence U*, and the standard deviation (of $\overline{U}$ and U*) are calculated.

3. Results and Discussion

3.1. Characteristics of the BRAD Sites

The hydrodynamic parameters inferred from the two ADVs for each site, as well as the topography variations measured with the SIS, are summarized in Table 2.

Sites 8, 9, and 10 are characterized by the presence of seagrass: The velocity values of $\overline{U}$ and U* can be considered to be influenced by the grass canopy and, thus, independent of the measurement height and topography of the bed [11]. Those values are not expected to follow the Law of the Wall and will not be considered for the rest of this study.

Table 2. Position, mean velocity, turbulence, and topography of the BRAD deployment sites.

Site	Latitude/ Longitude	Mean Velocity $\overline{U}$ (m/s)	Standard Deviation of $\overline{U}$ (m/s)	Turbulence U* (m/s)	Standard Deviation of U* (m/s)	Mean Zo (cm)	Standard Deviation of Seabed Elevation (cm)
1	39°54.594′; 008°29.532′	0.118	0.018	0.008	0.004	3.52	1.4
2	39°54.588′; 008°29.533′	0.072	0.018	0.010	0.004	3.13	1.7
3	39°54.600′; 008°29.526′	0.053	0.012	0.007	0.003	0.32	0.8
4	39°54.570′; 008°29.520′	0.098	0.020	0.011	0.007	0.39	0.8
5	39°54.564′; 008°29.532′	0.052	0.018	0.007	0.003	4.11	1.6
8	39°54.516′; 008°29.660′	0.023	0.007	0.005	0.003	5.22	1.1
9	39°54.528′; 008°29.663′	0.020	0.006	0.005	0.002	2.48	0.9
10	39°54.513′; 008°29.645′	0.011	0.004	0.003	0.001	0.77	1.1

Despite their remoteness from the study site, the wind speed and direction data measured at the Decimomannu Air Base (Latitude: 39°21.250′; Longitude: 8°58.333′) are considered representative of the wind regime in our study site. Indeed the Mistral wind dominates over the whole island, and is also the dominant wind regime in Cabras lagoon [25].

The sediment concentration in the water column is calculated for each site by averaging 5 to 9 water samples of one liter taken at varying depths (0.30 to 0.70 m) above the seabed. The concentration was always lower than 0.2 g/L (Table 1), justifying our initial assumption that drag reduction caused by turbidity can be considered negligible, and that the drag force felt by the flow is caused by the topographical bed roughness only. Three-dimensional images of the seabed have been created to estimate the roughness parameter.

Histograms of the variations in elevation from the mean are produced for selected subsections of proportionate sizes for each site (Figure 8). They have been de-trended, which means that any differential settling of BRAD into the bed has been removed. The histograms of elevation (Figure 8) are non-Gaussian, as the Shapiro-Wilk test rejects the hypothesis of a normal distribution for $\alpha = 0.05$ because of outliers in roughness, both negative and positive. Cumulative probability plots of elevation show these deviations from a normal distribution in the upper (largest) and lower (lowest) 5% of the elevation variation (Figure 9).

Rejection of the normality test is expected in the case of large samples, because significant results are derived even from small deviations from a normal distribution [36]. In our case, isolated features such as footprints can produce outliers, both positive and negative. Yet this should not prevent a statistical analysis. Indeed, when samples consist of several hundred measurements, as is the case here, their distribution can be ignored when performing parametric tests [36]. Furthermore, visual observation

shows that 85% of the data points follow the normal distribution (Figure 9), justifying that statistical parameters such as the standard deviation are applicable to assess the topographical bed roughness.

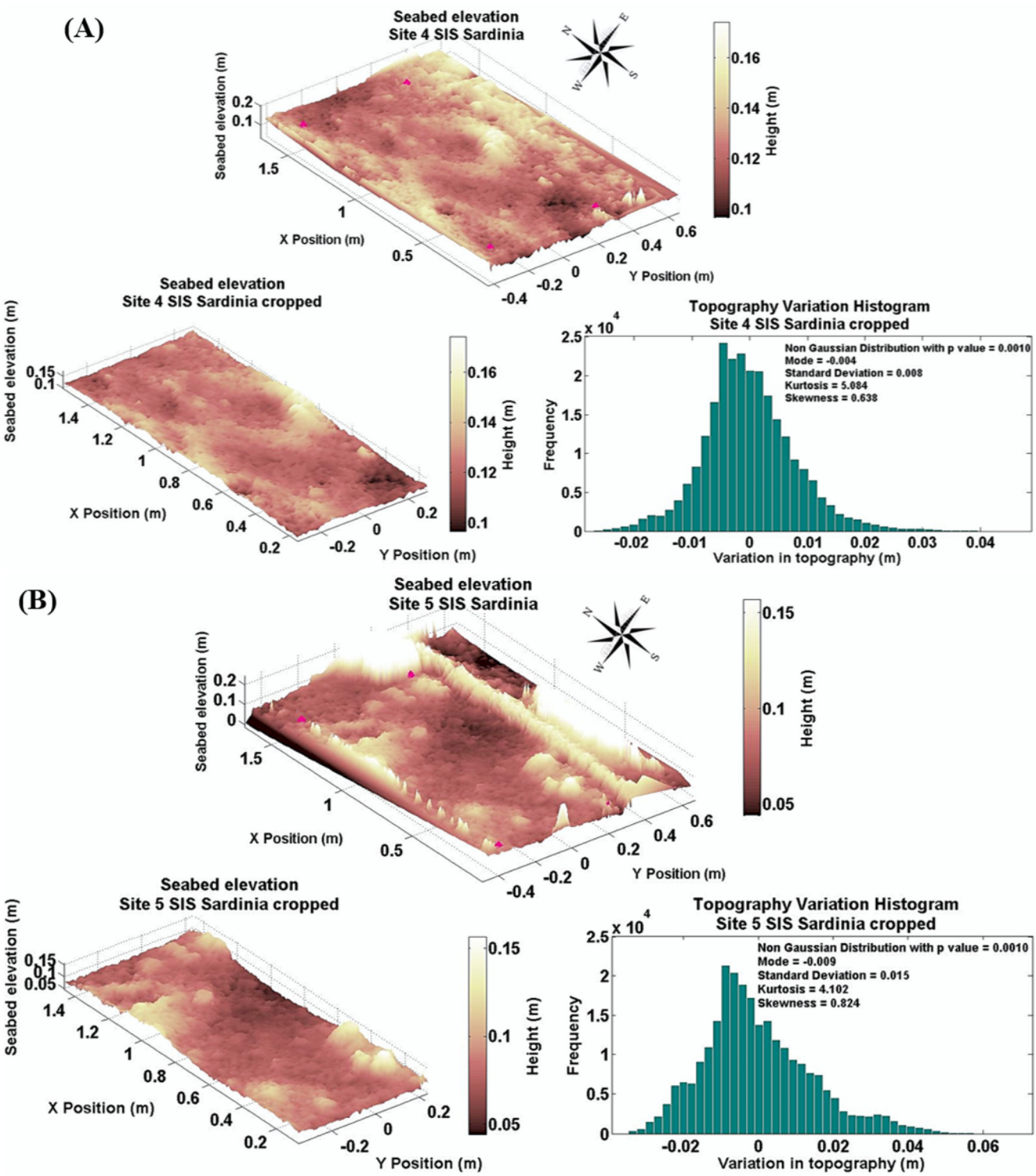

Figure 8. *Cont.*

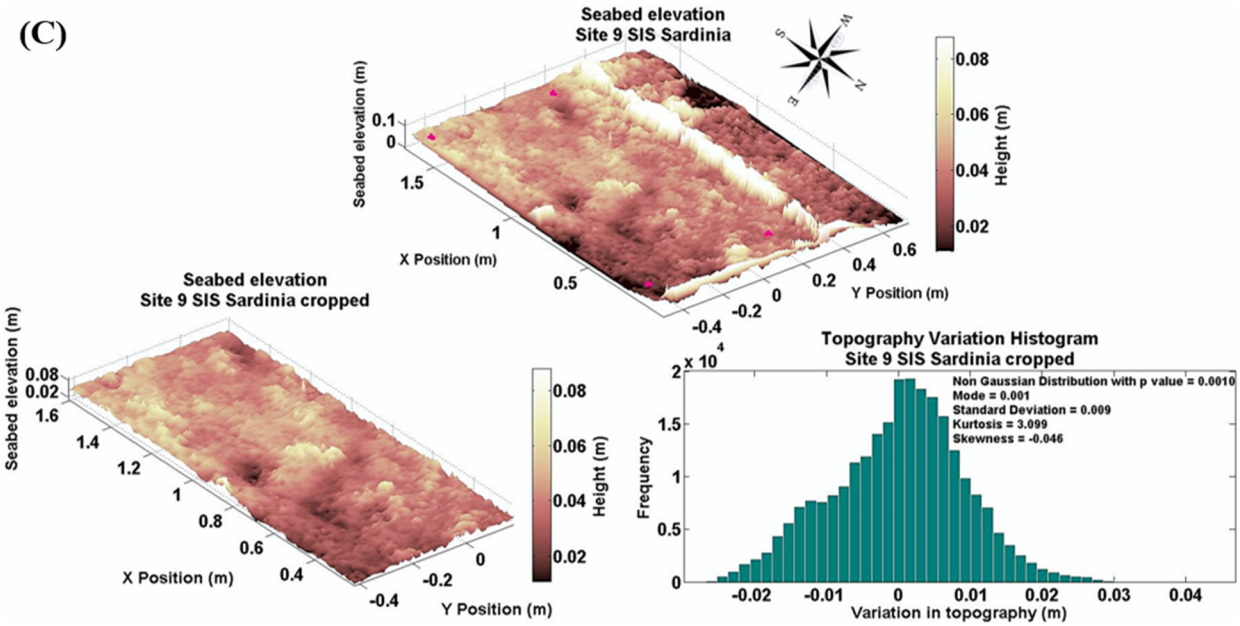

Figure 8. (**A**) Statistical analysis of seabed topography for site 4 as an example of BRAD output; (**B**) Statistical analysis of seabed topography for site 5 as an example of BRAD output; (**C**) Statistical analysis of seabed topography for site 9 as an example of BRAD output.

The topography images provide valuable visual information about the characteristics of the seabed: while site 4 displays ripple-like bed features, the topography at sites 5 and 9 is less regular. Observations on site suggest that those bed features correspond to serpulid reefs for site 5 and patches of seagrass for site 9. Most of the topography variations observed were about 4 cm in relief, though some features were 10 cm in height (site 5, Figure 8).

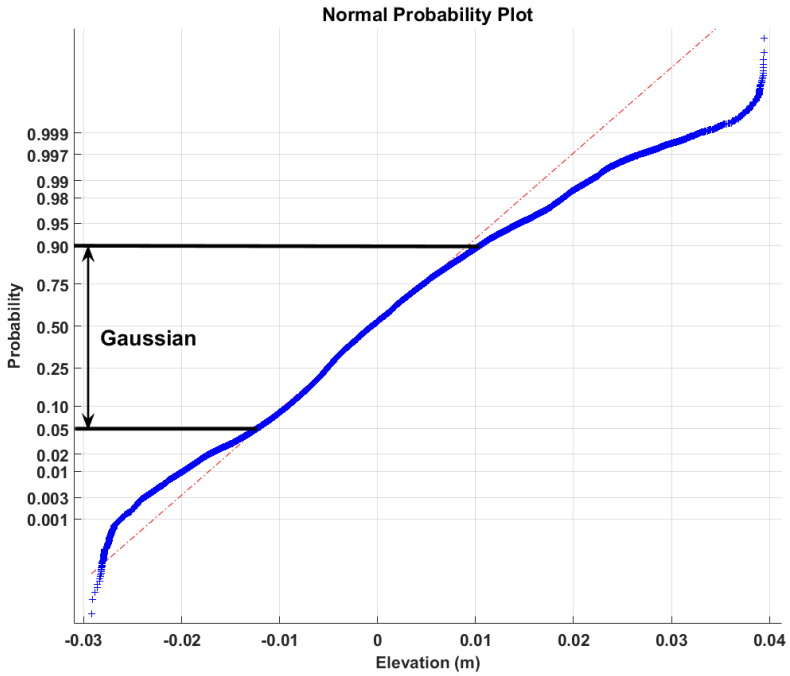

Figure 9. A probability plot of elevation data from site 4. The normal distribution is shown as the dotted-dashed line.

3.2. Relationship between Ks and Zo

The topography variation histograms are used to find the statistical parameters needed to estimate Ks, the topographical bed roughness. Based upon the work of Nikuradse (Equation (1)), it was expected that the bed roughness Ks from BRAD would be linearly correlated to Zo. The parameterization of topographical bed roughness as a function of roughness elements height has been tested in previous studies over oyster reefs [37]. Rather than bed form height, we define Ks as twice the standard deviation of the de-trended topography distribution. This definition corresponds to the mean height of 68% of the roughness elements in each sub-section. It gives a better measure of the bed roughness than the bed form heights as it is determined more directly in heterogeneous beds [23].

In order to account for the limiting scenario of a smooth bed, the skin friction factor K_{skin} is included in Equation (14). K_{skin} represents the frictional drag of a smooth bed, and is not considered significant compared to the effect of the bed features in the present case: It has been estimated from Nikuradse for constant Zo = 10^{-4} m after Thompson [10].

$$\mathrm{Ks} = 2 * \mathrm{STD} + \mathrm{Kskin} \quad (14)$$

The topographical bed roughness is plotted against the roughness length Zo to test the linearity of the correlation between the two parameters. The heterogeneity of the elevation measurements due to the resolution of the SIS are plotted as horizontal whiskers. Laboratory tests from previous studies have established a sub-centimetrical vertical resolution and a horizontal resolution of 2 cm, so the heterogeneity of measurement is defined as 2 cm [11]. The uncertainties of Zo, due to the variation in flow conditions over each 2 h experiment are plotted as vertical error bars.

The coefficient of determination R^2 of the plot is 0.93 and the p-value is 0.02 for $\alpha = 0.05$ (Figure 10). Since the p value is less than α, it is concluded that the linear correlation between the roughness length and the topographical bed roughness is statistically significant despite the limited number of data points.

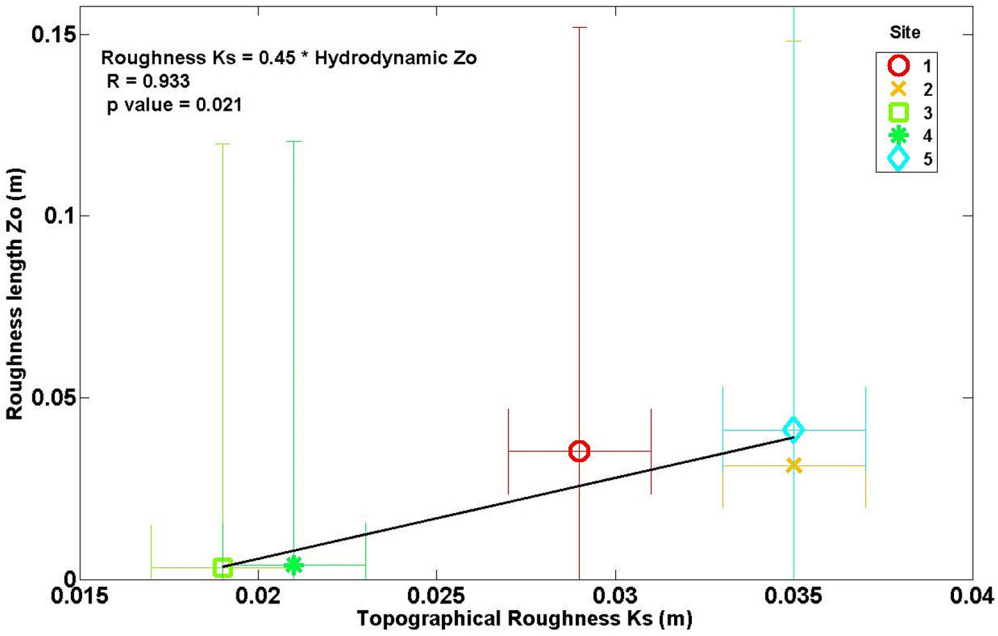

Figure 10. Correlation between the roughness length Zo and the topographical roughness Ks defined as 2*STD + skin friction.

This linear correlation indicates that Zo is indeed a function of the topographical bed roughness Ks: Soulsby's definition of the Reynolds number [18] then accounts for the total drag of the bed (Equation (4)), even though it is calculated exclusively from hydrodynamic factors. The field data that are not affected by seagrass patches fit on the transitional state between the viscosity dominated linear curve and the turbulence dominated logarithmic curve of the Law of the Wall for a factor $x = 0.5$ (Figure 11).

Figure 11 shows fits of the data at sites 1 to 5 to the concepts of boundary layer flow under laminar (linear blue line) and turbulent (log-linear red line) flows on the Clauser plot. The slope of the turbulent (red) fit is fixed as a constant (1/k). Note that our data are scattered about this fit for stations 2 to 5 (turbulent throughout the time series). Site 1, by contrast, appears to fluctuate between the laminar and turbulent regimes. The flow for this site is shown in Figure 7. Note the strong variations in mean flow between almost still water and 0.3 m/s. Laminar conditions would be expected to prevail close to still water, whereas the turbulent response would be expected at peak flows.

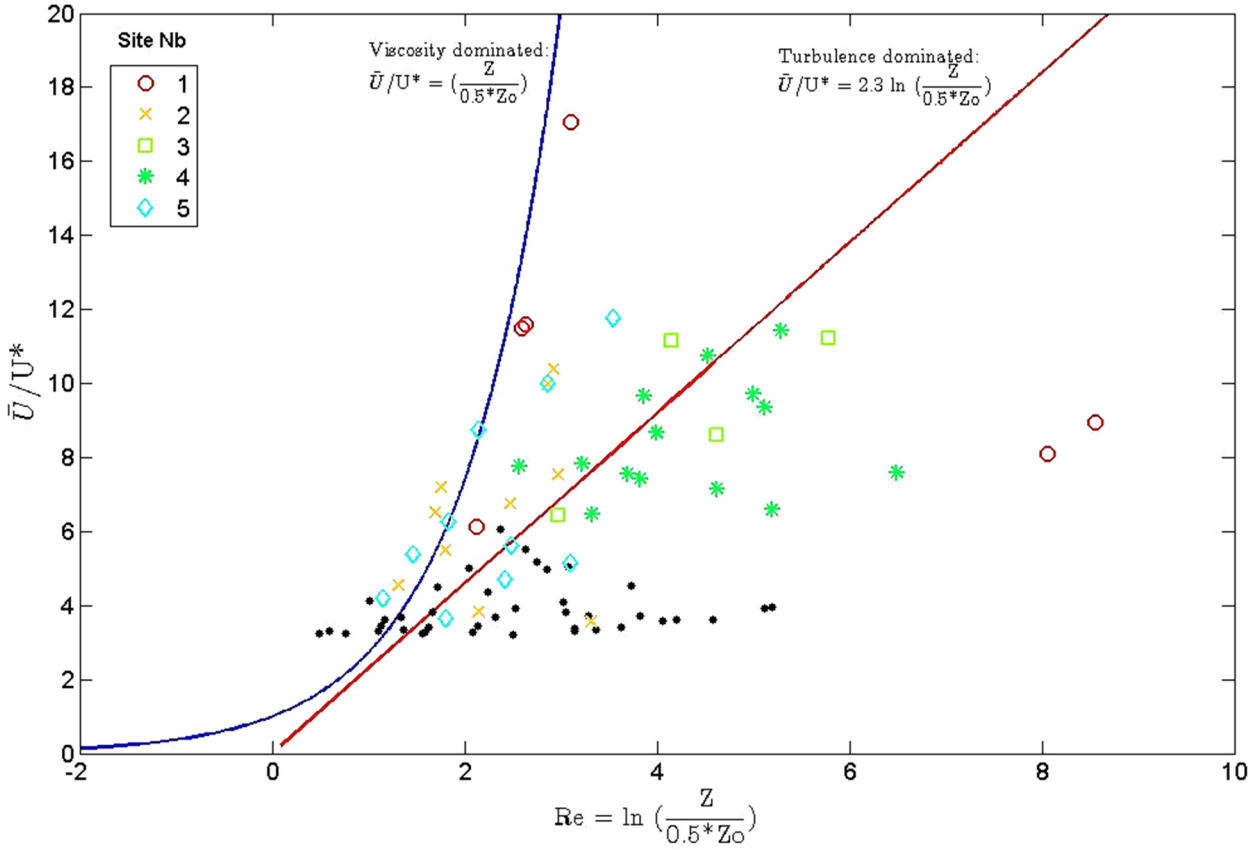

Figure 11. Fits of the data at sites 1 to 5 to the concepts of boundary layer flow under laminar (blue line) and turbulent (red line) flows on the Clauser plot. Black dots represent data from sites 8 to 10, characterized by the presence of seagrass.

3.3. Interpretations and Limits

The Law of the Wall is found to be valid for shallow environments characterized by a heterogeneous seabed in the absence of seagrass, provided that a factor $x = 0.5$ is added to our definition of Re. This factor is lower than those found in previous field surveys [18,19]. An x factor lower than the laboratory parameter $x = 9$ [18] means a higher Reynolds number at a given flow velocity, implying that

turbulence-dominated flows will occur at higher Reynolds numbers. This agrees with previous observations that the boundary between transitional and rough flows is related to bedforms, with fully-rough regimes occurring at higher Reynolds number for complex beds [33].

In order to study the effect of irregular bed features on the hydrodynamics of the benthic boundary layer, the Nikuradse relation between the topographical bed roughness Ks and the hydrodynamic roughness length Zo has been tested in the field using a simplified estimate of Ks. The factors of uncertainty for both parameters will be explored in this section.

Our definition for Ks takes into account the limit scenario of a smooth bed, when the standard deviation of the elevation variation tends toward 0; in this case the skin friction factor accounts for the entirety of the topographical bed roughness. The distribution and orientation of the roughness elements are not considered. This is deemed reasonable in our case as no clear orientation of bed roughness can be observed, with bed features consisting mainly of serpulid reefs and seashells (Table 1). It is also in accordance with previous studies on slope distributions over a 0.25 m^2 area, which have shown biogenic bed configurations to be isotropic [21].

Bed features change over time according to complex interactions between the current and the morphology of the bed: However, as long as the study is done over short time scales, it is reasonable to assume that Ks is static. Similarly, sediment transport and sedimentation processes are ignored, even though studies suggest that sediment accumulation reduces near-bed turbulence [38]. In all the stations considered, the sediment concentration is lower than 0.2 g/L (Table 1), so ignoring those two factors is reasonable.

Another factor influencing seabed roughness is the mean grain size and sorting. In our case, since the BRAD SIS only detects the topography, there is no information of bed material in the definition of Ks. The mean sediment type in Cabras lagoon is silty clay with 90% mud content according to previous studies [39], but this estimation does not represent accurately the complex bed near the inlet gate characterized by shelly mud or sand (Table 1). Nonetheless a wide range of roughness elements, including seashells, serpulid tubes or bed forms can be detected, due to to the high resolution of BRAD, providing a good representation of the complex bed characteristics of the deployment sites.

Bearing in mind these approximations, BRAD can be used in the calculation of a reliable estimate of Ks at a horizontal spatial resolution of 2 cm, which is sufficient to include most bed features.

The values for Zo, however, were extrapolated from local velocity profiles. The use of the Law of the Wall assumes that the flow is fully developed, stationary, uniform, and turbulent so it can be related to roughness. Yet some heterogeneity is observed in the velocity values, partially mitigated by the selection of eight minute intervals (Figure 7). Furthermore, measurements were taken at only two depths. These two factors result in a large uncertainty due to time variability in the roughness length values (Figure 10). Adding a third ADV to the frame for future studies should make the results more reliable.

Yet the Zo values found remain consistent with previous studies (Figure 12). The low Reynolds numbers observed indicate that most of our data are in the transitional regimes rather than in the fully rough region. In some sites, abnormally low Reynold numbers can be explained by the presence of seagrass, which attenuates currents [11] and wave energy [40]. In particular, sites 8, 9, and 10 have similar mean velocity and turbulence values, which are significantly lower than at the other sites (Table 2). The presence of seagrass explains why the roughness length at these sites is independent of the topographical bed roughness, and why the flow conditions do not follow the Law of the Wall.

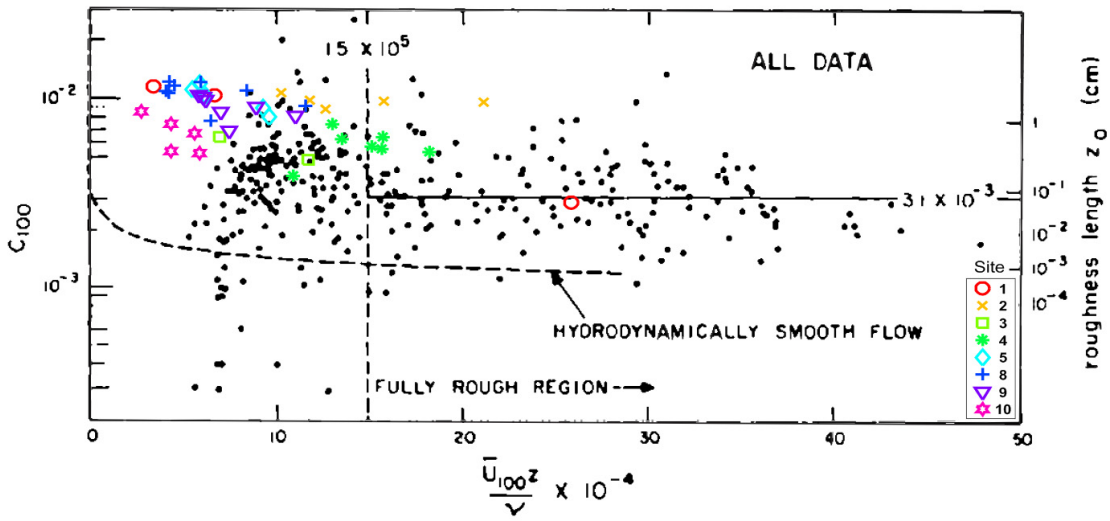

Figure 12. Comparison with Zo values from Sternberg [34] in various locations within Puget Sound [1] (modified from Sternberg [34]). The Reynolds number used for this graph is measured at 100 cm above the seabed (sea axis label).

According to the results in Figure 12, most of our observations were made under turbulent smooth conditions. The existence of a linear correlation between Ks and Zo indicates that the topographical bed roughness has an influence on the mean velocity profile in the lower part of the benthic boundary layer. The effect of topographical roughness on near-bed velocity has already been observed in the case of hydraulically rough flows over gravel beds [41] and over oyster reefs [37].

For this to occur, however, a proportion of the roughness elements must be larger than the viscous sublayer that is present near the bed under turbulent smooth conditions. This begs the question: what proportion of the roughness elements are protruding through the viscous sub-layer in order to exert influence on the flow? This intermediate state where Ks starts impacting the velocity profile is referred to as the transitional state and is accompanied by a buffer layer in the vertical profile [1]. It will however be necessary to test the validity of the obtained equation in turbulent rough conditions: The correlations in Figure 11 should be more significant than in the transitional state because of the absence of a viscous sublayer.

The linear relation between Ks and Zo is however very different from Nikuradse's results, where Zo is 30 times smaller than Ks: By contrast, Zo is larger than the mean size of the roughness elements in our case (Figure 10). Pinpointing the factor that predominantly influences Zo in the field is problematic, as not all parameters can be monitored. We suggest that the abnormally high roughness length is due either to the weak flows characteristic of the study site, in a location affected by man-made structures, such as the flood protector dykes and fish barriers, or to the heterogeneity of the seabed. Indeed at this measurement scale, the flow could be influenced by the higher bed features rather than by the most frequent ones. The presence of small-scale bedforms seems to affect the relation between roughness length and topographical bed roughness.

3.4. Future Development

BRAD is a high-resolution acoustic system developed at the National Oceanography Centre Southampton. With a horizontal resolution of 2 to 3 cm [13], this instrument allows for an accurate

representation of the topographical bed roughness: in our site in Cabras lagoon, the topography variations typically range between 3 and 10 cm. In the case of digital terrain models created from multibeam echosounder data, the error caused by the interpolation process reaches 5 cm for a smooth surface and 10 cm for a more complex seabed [42]. Multibeam echosounder data are also typically collected with vessels [20], making BRAD more suitable to shallow-water environments surveying, though at the cost of a smaller coverage (Figure 4B).

BRAD, therefore, provides more reliable measurements for the calculation of the topographical bed roughness for complex beds in shallow-water environments, where the applicability of the Nikuradse relation needs to be further investigated. The elevation maps obtained from acoustic profilers have been considered suitable for statistical roughness analysis by previous studies, even though DEMs from improved stereophotogrammetric setups have yielded better results [24]. Furthermore, compared to the latter method, this instrument allows for a simultaneous measurement of the bed roughness and flow conditions, providing additional arguments to relate the topographical bed roughness to hydrodynamic parameters [23]. The current setup of BRAD can be improved by adding one or several ADVs to the BRAD frame in order to increase the reliability of our roughness length estimates.

The data processing method proposed in this study is semi-automatic and operates in a Matlab environment: This favors high reproducibility. Though the dataset used herein is small, it can be easily extended to other sites. This would test the universality of our relationship, or whether different factors must be used for different locations.

4. Conclusions

The study tested a reproducible method for assessing the influence of the topography on the turbulent state in the benthic boundary layer. To that end, the topographical bed roughness Ks and the roughness length Zo were estimated independently using a seabed mapping system BRAD and two near-bed ADVs.

A proxy of the topographical bed roughness is proposed using statistical parameters of the elevation variations. A statistically-robust relationship has been obtained between Zo and Ks when defining $Ks = 2*STD + K_{skin}$ with STD being the standard deviation of the seabed elevation variations and K_{skin} the skin friction caused by a smooth bed. This simple relationship makes it possible to compare the Reynolds numbers in areas characterized by different topographies and sediment properties. In the case of Cabras lagoon, the values collapse on the logarithmic curve of the Clauser plot by changing the Soulsby fitting factor [18] from 9 to 0.5. This variation is thought to be linked to the higher complexity of the bed compared to laboratory experiments. It also shows the applicability of the Clauser plot to sites characterized by irregular bed features.

Acknowledgments

Funding for this project came from RITMARE, the Italian National programme of scientific and technological marine research (subproject 3, package 4, action 5). We thank Geoffrey Barre for his hard work during the field campaign, Alanoud Al-Ragum for the backscatter attenuation method, and Johann Schnyder for co-supervising part of this project.

Author Contributions

Carl L. Amos, Hachem Kassem, Georg Umgiesser and Andrea Cucco collected the dataset. Alice Lefebvre, Carl L. Amos and Hachem Kassem tested the BRAD instrument. Clémentine Chirol processed the data. Clémentine Chirol and Carl L. Amos interpreted the data. Alice Lefebvre provided analysis tools. Clémentine Chirol wrote the paper with comments from Carl L. Amos, Hachem Kassem and Alice Lefebvre.

Conflicts of Interest

The authors declare no conflict of interest.

References

1. Komar, P.D. Boundary layer flow under steady unidirectional currents. In *Marine Sediment Transport and Environmental Management*; Jonh Wiley & Sons: New York, NY, USA, 1976; pp. 91–106.
2. Dyer, K.R. *Coastal and Estuarine Sediment Dynamics*; Wiley: Chichester, UK, 1986; pp. 1–195.
3. Villacieros-Robineau, N.; Herrera, J.L.; Castro, C.G.; Piedracoba, S.; Roson, G. Hydrodynamic characterization of the bottom boundary layer in a coastal upwelling system (Ria de Vigo, NW Spain). *Cont. Shelf Res*. **2013**, *68*, 67–79.
4. Clauser, F.H. The turbulent boundary layer. *Adv. Appl. Mech*. **1956**, *4*, 1–51.
5. Heathershaw, A. The turbulent structure of the bottom boundary layer in a tidal current. *Geophys. J. Int*. **1979**, *58*, 395–430.
6. Thompson, C.E.L.; Amos, C.L.; Angelaki, M.; Jones, T.E.R.; Binks, C.E. An evaluation of bed shear stress under turbid flows. *J. Geophys. Res*. **2006**, *111*, 1–8.
7. Best, J.L.; Leeder, M.R. Drag reduction in turbulent muddy seawater flows and some sedimentary consequences. *Sedimentology* **1993**, *40*, 1129–1137.
8. Amos, C.L.; Feeney, T.; Sutherland, T.F.; Luternauer, J.L. The stability of fine-grained sediments from the Fraser River Delta. *Estuar. Coast. Shelf Sci.* **1997**, *45*, 507–524.
9. Cloutier, D.; LeCouturier, M.N.; Amos, C.L.; Hill, P.R. The effects of suspended sediment concentration on turbulence in an annular flume. *Aquat. Ecol*. **2006**, *40*, 555–565.
10. Thompson, C.E.L. The Role of the Solid-transmitted Bed Shear Stress of Mobile Granular Material on Cohesive Bed Erosion by Unidirectional Flow. Ph.D. Thesis, University of Southampton, Southampton, UK, 2003; pp. 1–214.
11. Lefevbre, A. Bed Roughness over Vegetated Beds: Sonar Imaging Techniques and Effect on Unidirectional Currents. Ph.D. Thesis, University of Southampton, Southampton, UK, 2009; pp. 1–232.
12. Burchard, H.; Craig, P.D.; Gemmrich, J.R.; van Haren, H.; Mathieu, P.-P.; Meier, H.E.M.; Smith, W.A.M.N.; Prandke, H.; Rippeth, T.P.; Skyllingstad, E.D.; *et al*. Observational and numerical modeling methods for quantifying coastal ocean turbulence and mixing. *Prog. Oceanogr*. **2008**, *76*, 399–442.

13. Lefebvre, A.; Lyons, A.P.; Thompson, C.E.L.; Amos, C. A new system for seafloor characterisation: BRAD, the Benthic Roughness Acoustic Device. In Proceedings of the International Conference on Underwater Acoustic Measurements: Technology and Results, Southampton, UK, 21–26 June 2009; pp. 1–8.
14. Nelson, T.R. Benthic Boundary Layer Processes: Bedform Evolution and Bottom Turbulence. Ph.D. Thesis, University of South Carolina, Columbia, SC, USA, 2013; pp. 1–244.
15. Nikuradse, J. *Strömungsgesetze in Rauhen Rohren*; VDI-verlag: Düsseldorf, Germany, 1933.
16. Liu, Z. *Sediment Transport*; Aalborg Universitet: Copenhagen, Denmark, 2001; pp. 54–56.
17. Middleton, G.V.; Southard, J.B. Mechanics of sediment movement. In *Society of Economic Paleontologists and Mineralogists*; California University: Los Angeles, CA, USA, 1984; pp. 1–401.
18. Soulsby, R.L. The bottom boundary layer of shelf seas. *Elsevier Oceanogr. Ser.* **1983**, *35*, 189–266.
19. Chriss, T.M.; Caldwell, D.R. Universal similarity and the thickness of the viscous sublayer at the ocean floor. *J. Geophys. Res*. **1984**, *89*, 6403–6414.
20. Guerrero, M.; Lamberti, A. Flow field and morphology mapping using ADCP and multibeam techniques: Survey in the Po River. *J. Hydraul. Eng*. **2011**, *137*, 1576–1587.
21. Wheatcroft, R.A. Temporal variation in bed configuration and one-dimensional bottom roughness at the mid-shelf STRESS site. *Cont. Shelf Res*. **1994**, *14*, 1167–1190.
22. Nikora, V.I.; Goring, D.G.; Biggs, B.J.F. On gravel-bed roughness characterization. *Water Resour. Res.* **1998**, *34*, 517–527.
23. Aberle, J.; Nikora, V.; Henning, M.; Ettmer, B.; Hentschel, B. Statistical characterization of bed roughness due to bed forms: A field study in the Elbe River at Aken, Germany. *Water Resour. Res*. **2010**, *46*, 1–11.
24. Bertin, S.; Friedrich, H. Measurement of gravel-bed topography: Evaluation study applying statistical roughness analysis. *Am. Soc. Civil Eng*. **2014**, *140*, 269–279.
25. Ferrarin, C.; Umgiesser, G. Hydrodynamic modelling of a coastal lagoon: The Cabras lagoon in Sardinia, Italy. *Ecol. Model*. **2006**, *188*, 340–357.
26. De Falco, G.; Magni, P.; Teräsvuori, L.M.H.; Matteucci, G. Sediment grain size and organic carbon distribution in the Cabras lagoon (Sardinia, Western Mediterranean). *Chem. Ecol*. **2004**, *20*, 367–377.
27. Magni, P.; De Falco, G.; Como, S.; Casu, D.; Floris, A.; Petrov, A.N.; Castelli, A.; Perilli, A. Distribution and ecological relevance of fine sediments in organic-enriched lagoons: The case study of the Cabras lagoon (Sardinia, Italy). *Mar. Pollut. Bull*. **2008**, *56*, 549–564.
28. Simeone, S.; Cucco, A.; Como, S.; De Falco, G.; Magni, P.; Perilli, A. Sediment distribution and hydrodynamic patterns in the Cabras lagoon, Sardinia (Italy). In Proceedings of the 16th Meeting of the Italian Society of Ecology, Viterbo, Italy, 19–22 September 2006; pp. 1–6.
29. Moore, S.A.; Le Coz, J.; Hurther, D.; Paquier, A. On the use of horizontal-ADCPs for sediment flux measurements in rivers. In *Proceedings of the 34th World Congress of the International Association for Hydro-Environment Research and Engineering: 33rd Hydrology and Water Resources Symposium and 10th Conference on Hydraulics in Water Engineering*; Engineers Australia: Barton, Australia, 2011; pp. 3659–3666.
30. Goring, D.G.; Nikora, V.I. Despiking acoustic doppler velocimeter data. *J. Hydraul. Eng.* **2002**, *128*, 117–126.

31. Mori, N.; Suzuki, T.; Kakuno, S. Noise of acoustic doppler velocimeter data in bubbly flows. *J. Eng. Mech*. **2007**, *133*, 122–125.
32. Chanson, H.; Trevethan, M.; Koch, C. Discussion of "Turbulence Measurements with Acoustic Doppler Velocimeters" by Carlos M. García, Mariano I. Cantero, Yarko Niño, and Marcelo H. García. *J. Hydraul. Eng*. **2007**, *133*, 1283–1286.
33. Sternberg, R.W. Friction factors in tidal channels with differing bed roughness. *Mar. Geol*. **1967**, *6*, 243–260.
34. Stapleton, K.R.; Huntley, D.A. Seabed stress determinations using the inertial dissipation method and the turbulent kinetic energy method. *Earth Surf. Process. Landf.* **1995**, *20*, 807–815.
35. Schlichting, H.; Gersten, K.; Gersten, K. *Boundary-Layer Theory*; Springer: New York, NY, USA, 2000; pp. 1–799.
36. Ghasemi, A.; Zahediasl, S. Normality tests for statistical analysis: A guide for non-statisticians. *Int. J. Endocrinol. Metab.* **2012**, *10*, 486–489.
37. Styles, R. Flow and turbulence over an oyster reef. *J. Coast. Res.* **2015**, *31*, 978–985.
38. Friedrichs, C.T.; Wright, L.D.; Hepworth, D.A.; Kim, S.C. Bottom-boundary-layer processes associated with fine sediment accumulation in coastal seas and bays. *Cont. Shelf Res.* **2000**, *20*, 807–841.
39. Molinaroli, E.; Guerzoni, S.; De Falco, G.; Sarretta, A.; Cucco, A.; Como, S.; Simeone, S.; Perilli, A.; Magni, P. Relationships between hydrodynamic parameters and grain size in two contrasting transitional environments: The Lagoons of Venice and Cabras, Italy. *Sediment. Geol*. **2009**, *219*, 196–207.
40. Manca, E.; Cáceres, I.; Alsina, J.M.; Stratigaki, V.; Townend, I.; Amos, C.L. Wave energy and wave-induced flow reduction by full-scale model Posidonia oceanica seagrass. *Cont. Shelf Res*. **2012**, *50–51*, 100–116.
41. Friedrich, H.; Spiller, S.M.; Rüther, N. Near-bed flow over a fixed gravel bed. In *River Flow*; Taylor & Francis: London, UK, 2014; pp. 1–279.
42. Maleika, W.; Palczynski, M.; Frejlichowski, D. Interpolation methods and the accuracy of bathymetric seabed models based on multibeam echosounder data. In *Intelligent Information and Database Systems*; Springer: Berlin, Germany, 2012; pp. 466–475.